Journal of Power Sources 242 (2013) 742–755

Contents lists available at SciVerse ScienceDirect

Journal of Power Sources

journal homepage: www.elsevier.com/locate/jpowsour

Optimal management of stationary lithium-ion battery system in electricity distribution grids

Arturs Purvins*, Mark Sumner

The University of Nottingham, Department of Electrical & Electronic Engineering, University Park, Nottingham NG7 2RD, United Kingdom

HIGHLIGHTS

- A battery management model is developed for stationary battery applications.
- The model is tested in a hypothetical case study in Great Britain in 2020.
- Battery usage ensures high wind energy surplus compensation in the distribution grid.
- Efficient battery utilisation is achieved.
- The battery contributes to residual demand smoothing at electricity market level.

ARTICLE INFO

Article history:
Received 28 February 2013
Accepted 18 May 2013
Available online 5 June 2013

Keywords:
Lithium-ion battery
Energy management
Energy storage
Demand shifting
Distribution grid
Smart grid

ABSTRACT

The present article proposes an optimal battery system management model in distribution grids for stationary applications. The main purpose of the management model is to maximise the utilisation of distributed renewable energy resources in distribution grids, preventing situations of reverse power flow in the distribution transformer. Secondly, battery management ensures efficient battery utilisation: charging at off-peak prices and discharging at peak prices when possible. This gives the battery system a shorter payback time. Management of the system requires predictions of residual distribution grid demand (i.e. demand minus renewable energy generation) and electricity price curves (e.g. for 24 h in advance).

Results of a hypothetical study in Great Britain in 2020 show that the battery can contribute significantly to storing renewable energy surplus in distribution grids while being highly utilised. In a distribution grid with 25 households and an installed 8.9 kW wind turbine, a battery system with rated power of 8.9 kW and battery capacity of 100 kWh can store 7 MWh of 8 MWh wind energy surplus annually. Annual battery utilisation reaches 235 cycles in per unit values, where one unit is a full charge-depleting cycle depth of a new battery (80% of 100 kWh).

1. Introduction

Lithium-ion energy storage technologies are attracting a great deal of interest in the field of battery[1] research for electric vehicles (EV). The interest in Lithium-ion batteries is based on several technical advantages: high energy conversion efficiency of more than 95% (electrical–chemical–electrical, at 1C[2] and below), a long lifecycle of 3000 cycles (at deep discharge of 80%) and high energy density up to 200 Wh kg^{-1} [1,2]. According to the technology roadmap of European Commission (EC) [3], it is expected that a large number of EVs will be using the electricity grid by 2020. This in turn stimulates research on Lithium-ion technologies, where efforts are focused on increasing technical performance and reducing costs in general. The latter is currently the main drawback [4], but as they overcome this barrier and given the above-mentioned characteristics, Lithium-ion batteries are suitable for large scale use not only in EVs but also in stationary applications.

Potential grid support services of battery technologies are widely studied mainly for grid connected EVs, but also for stationary battery applications. Battery energy storage as a means for facilitating distributed renewable energy sources of electricity (RES-E) penetration is the subject of a study by Leadbetter and Swan [5], who conclude that energy storage systems provide a

* Corresponding author. Tel.: +44 49 (0)1639 404.
E-mail addresses: arturs.purvins@nottingham.ac.uk, arturs.purvins@inbox.lv (A. Purvins).

[1] 'Battery' refers to a secondary electrochemical battery.

[2] 'xC' indicates battery charging/discharging current rate, e.g., charging current of 1 C for a 5 Ah battery is 5 A.

0378-7753/$ – see front matter © 2013 Elsevier B.V. All rights reserved.
http://dx.doi.org/10.1016/j.jpowsour.2013.05.097

means of increasing grid flexibility and enabling the integration of stochastically variable generation sources by temporarily decoupling this generation from demand. White and Zhang [6] find that the importance of EVs lies in peak demand reduction on a daily basis; however, there is little financial incentive. According to Denholm et al. [7], EV batteries are also able to reduce curtailment under high RES-E generation. In all these studies, batteries are seen as a controllable load, which, when available, can be shifted to accommodate variable RES-E power. For example, a battery could be charged at high RES-E generation and low demand in the distribution grid in order to prevent situations of reverse power flow in the distribution transformer. In order to increase the feasibility of grid connected batteries, it is suggested that load shifting be shared with other grid support services such as frequency regulation [8] and voltage control [9]. Neubauer and Pesaran [10] have studied the secondary use of EV batteries as grid based energy storage applications, which has the potential to become a common component of automotive batteries' lifecycle, essential for use in cost effective energy storage. The abovementioned grid support services of battery systems are supported by the EC as one of the key policy priorities for renewable energy generation, including the development of methods and tools for the network integration of distributed renewable resources [11].

Given the energy technology trends in distribution grids and the importance of feasibility for the widespread implementation of batteries, this article puts forward proposals as to how a Lithium-ion battery system[3] can be best managed for stationary applications. The proposals are aimed at maximum feasibility of battery systems, focussing on the following three priorities (in order of importance):

1) High utilisation of distributed RES-E in the distribution grid

The battery is managed so as to prevent reverse power flows in the distribution transformer. At high RES-E penetration, this may avoid the need for reinforcements of the distribution grid.

2) Efficient utilisation of the battery

Efficient utilisation of batteries leads to a short payback period. This is an important economic incentive from the end energy user perspective, as it could result in high battery deployment in households. Moreover, since battery operation mode is regulated by electricity price, the battery contributes to the smoothing of residual demand (i.e. demand minus RES-E generation) at electricity market level. Demand smoothing is a process in which demand variations are reduced by charging and discharging batteries at times of low and high demand respectively. This operation follows the prices of the electricity market.

3) Smoothing of residual distribution grid demand (i.e. demand minus RES-E generation)

Residual demand smoothing in the distribution grid will lead to peak demand reductions when the electricity price is high and to off-peak demand rises when the price is low. This smoothing is performed for an aggregated residual distribution grid demand at step-down distribution transformer level, which is the product of distribution grid demand minus distributed generation (DG) from RES-E. Dynamic grid support services like frequency and voltage control are beyond the scope of this article.

[3] 'Battery system' refers to battery and power converter.

The proposed approach to management is based on the demand-tracking management model of a battery for stationary applications presented by Purvins et al. [12]. The aim of demand-tracking management is peak demand shaving and demand smoothing. The proposed approach includes additional management priorities and is more accurate, since it takes account of battery aging, which causes reduction of battery capacity and efficiency after any additional charge-depleting cycle. Moreover, the proposed management code would be more efficient for distribution grid applications, as it recalculates optimal battery operating power at hourly intervals, taking into account updated prediction profiles of residual distribution grid demand and electricity market price. The management can be applied for new as well as second-hand battery systems.

Section 2 of the article describes the battery system management model in details. In Section 3, a case study in Great Britain (GB) is presented, starting with demand and wind speed data acquisition and proceeding with wind farm/turbine power calculations, battery system sizing and study results. In Section 4, the payback period of the battery system is calculated at different battery system capital costs and electricity prices. Section 5 contains our overall conclusions.

2. Management methodology

The battery system is managed according the three abovementioned priorities: high utilisation of distributed RES-E in the distribution grid (1st priority), efficient utilisation of the battery (2nd priority) and residual distribution grid demand smoothing (3rd priority).

In line with the first priority, battery capacity is firstly reserved to be used to prevent reverse power flows in the distribution grid transformer, i.e. the battery stores RES-E energy surplus in the distribution grid and supplies the stored energy to the grid during high residual demand.

The second priority, efficient utilisation of the battery, is achieved by charging the battery during times of low electricity price and discharging during high price periods when possible. The battery thus reaches the highest possible state of charge (SoC) at the end of the low electricity price period. At the beginning of the next high price period, this stored energy is supplied to the grid when possible. The minimum possible SoC is thus reached at the end of the high price period. The highest and lowest possible SoCs are assumed to be 100% and 20% respectively. However, since battery performance is limited by the rated battery system power, management constraints and the length of the low/high price periods, the highest/lowest SoCs will not always be reached. Nowadays, with different electricity price systems, low electricity prices usually apply during the night at times of off-peak demand and high electricity prices during peak demand hours (morning and afternoon peak). In the future, with electricity systems at high RES-E deployment, the electricity price curve may change its characteristics and be partly determined by RES-E generation. In Great Britain, electricity price levels may be strongly influenced by overall country-scale wind farm generation. At the end of 2011, Great Britain already had 6.5 GW installed wind farm capacity [13] and, according to the national renewable energy action plan, will have 27.9 GW by 2020 [14]. High wind generation during midday may reduce residual demand significantly, leading to a change in electricity price from high to low. This electricity price will determine the operation mode of the battery.

Finally, battery system operation (instantaneous) power is variable and this allows for residual demand smoothing at distribution grid level. Thus, during times of high electricity prices, battery capacity is firstly reserved for the reduction of the highest residual

demand. Similarly, during times of low prices, the lowest residual demand is to be increased first by charging the battery.

2.1. Management model

This sub-section presents the battery system management model, which follows the principles of the demand-tracking model described by Purvins et al. [12], the main differences being additional priorities for battery management (see above) according to which the optimal battery system rated power and operation mode is calculated. In addition, the proposed model takes into account battery aging. The management model is set out in MS Excel Visual Basic computer language.

The management timescale is one hour, which is considered to be adequate, because (i) the management accuracy depends on the timescale and prediction precision both of the residual distribution grid and electricity market price profiles for the next 24 h and (ii) the battery contributes to the smoothing of aggregated residual distribution grid demand, which is already partly smoothed. So, further reducing the timescale will not make a significant difference.

Battery management is thus calculated for every hour. At the beginning of each hour (e.g. at 00:00 am, then at 01:00 am, and so on), the optimal battery system rated power and operation mode are calculated. These operation conditions are applied for the battery system until the end of the hour. When the next hour starts, the conditions are recalculated. For this calculation, the following input data are required (see Fig. 1):

- predicted residual distribution grid demand profile one day in advance, with hourly intervals ($Demand = [dem_i]_{1\times24}$)
- predicted price profile one day in advance, with hourly intervals ($Price = [price_i]_{1\times24}$), indicating high and low price hours
- the rated power of the battery system (P_{rated})
- actual internal resistance of the battery (R_{actual})
- actual battery capacity (C_{actual})
- charging losses in the battery (η_{charge})
- discharging losses in the battery (η_{disch})
- losses in the AC/DC ($\eta_{AC/DC}$) electrical-power conversion process
- losses in the DC/AC ($\eta_{DC/AC}$) electrical-power conversion process
- the actual SoC of the battery (q_{actual})
- maximum annual residual demand (Dem_{max})
- calculation step ($Step$)

The last factor determines the calculation accuracy. The smaller the *Step*, the more precise is the calculated value. The *Demand* array contains residual demand values (i.e. demand minus RES-E generation). The *Price* array contains information on the electricity price: value '1' indicates low price and value '2' indicates high price. Predicted residual demand and price profiles are used for calculating the optimal battery system rated power for the current hour. These profiles, as well as actual battery SoC, are to be updated every hour. The battery's internal resistance is expressed in per unit values, where the base unit is the resistance of a new battery. Resistance will increase due to battery aging. Battery capacity is another parameter affected by battery aging. Capacity is reduced by battery utilisation. R_{actual} and C_{actual} are recalculated after any charge-depleting cycle of the battery.

Firstly, the model forms the following data arrays: $Charge = [charge_{k.m}]_{2\times24}$, $Disch = [disch_{k.m}]_{2\times24}$ and $Q = [q_r]_{1\times24}$. Initially, all entries in the *Charge* and *Disch* arrays are set to zero and all entries in the *Q* array are set at the q_{actual} value. The *Charge* and

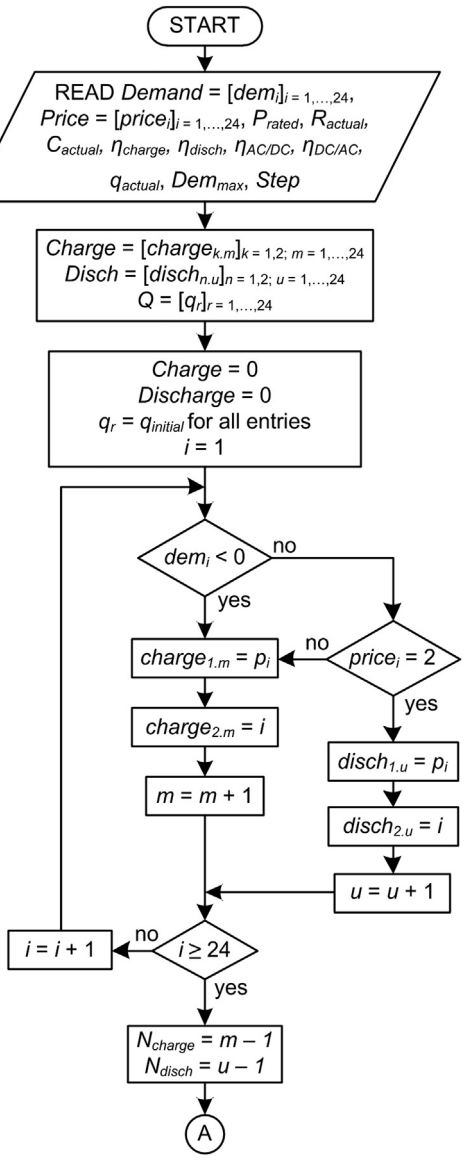

Fig. 1. Flowchart of battery system management model (part 1 of 2).

Disch arrays at the end of the calculation will contain information about the smoothed residual demand data in the distribution grid. The battery's SoC for any hour of the day during the battery utilisation process will be registered in the *Q* array.

In line with the flowchart, the values of the *Demand* array are split into the *Charge* and *Disch* arrays according the operation mode of the battery. The operation mode is determined by the entries in the *Demand* and *Price* arrays. During hours of energy surplus (RES-E generation higher than demand), the battery operates in charging mode. At other times, the charging mode is determined by low electricity prices and the discharging mode by high prices. Residual demand values appear in the first row of the *Charge* and *Disch* arrays, whereas the second row contains the serial number of the column of the *Demand* array, which indicates the number of the hour in the profile. For example, number one indicates that it is the first hour in the profile (not the time of day). The quantity of records in the *Charge* and *Disch* arrays is registered in N_{charge} and N_{disch} respectively.

By way of illustration, representative 24 h residual distribution grid demand and price profiles are shown in Fig. 2. The acquisition

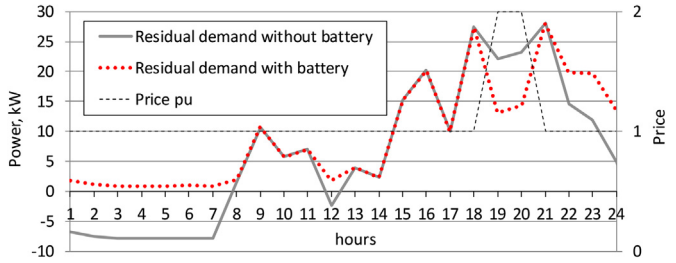

Fig. 2. Representative residual demand with and without battery and price profiles for one day.

of these profiles will be explained later in Section 3, where the specific case study is presented. The battery system applied in this representative case has rated power of 8.9 kW and battery capacity of 100 kWh. Negative residual demand indicates RES-E generation surplus in the distribution grid. Entries for residual demand and price profiles are presented in Table 1 in the *Demand* and *Price* arrays respectively. In the *Q* array, all entries are 20 kWh, which is the minimum SoC. This indicates that battery SoC at the beginning of hour one (q_{actual}) is 20%. The *Charge* and *Disch* arrays contain residual demand values and the number of the hour for charging and discharging operation modes respectively.

The flowchart continues in Fig. 3 with the columns in the *Charge* and *Disch* arrays arranged in descending order, so that the smoothing of the residual demand profile starts simultaneously by increasing the lowest residual demand value in the *Charge* array and decreasing the highest residual demand value in the *Disch* array. Battery SoC (q_r) is registered in the *Q* array accordingly. In the *Charge* array, residual demand is increased by $Step/\eta_{AC/DC}/(1-(1-\eta_{charge})^{*}R_{actual})$. Due to the battery charging, battery SoC (q_r) is increased by *Step* for the hour in which the battery is charged and beyond. This represents battery charging. Residual demand in the *Disch* array is decreased by $Step^{*}\eta_{DC/AC}{}^{*}(1-(1-\eta_{disch})^{*}R_{actual})$. The SoC ($q_r$) is now decreased by *Step* for the hour in which the battery is discharged and beyond. After this smoothing step, the following conditions are checked:

1. Battery system rated power and maximum annual residual demand is not exceeded in the hours of charging at low electricity price (i.e. $charge_{1.m} - dem_i \leq P_{rated}$ and $charge_{1.m} \leq Dem_{max}$).
2. RES-E surplus at high electricity price is not overcompensated (i.e. $charge_{1.m} \leq 0$).
3. Battery system rated power is not exceeded and zero residual demand is not violated in the hours of discharging (i.e. $dem_i - disch_{1.u} \leq P_{rated}$ and $disch_{1.u} \geq 0$).
4. The available battery capacity C_{actual} is not exceeded (i.e. $q_r \leq C_{actual}$).
5. The battery's minimum SoC is not violated (i.e. $q_r \geq 0.2$).

If all the conditions are met, the *Charge* and *Disch* arrays are arranged again in descending order and the cycle is repeated. However, if conditions #1 or #2 are not met, then the changes performed in the last smoothing cycle involving the *Charge* array and consequently the relevant entries in the *Q* array are cancelled. Then smoothing continues with the next lowest entry in the *Charge* array. If condition #3 is not met, then the changes performed in the last smoothing cycle involving the *Disch* array and consequently the relevant entries in the *Q* array are cancelled. Then smoothing continues with the next highest entry in the *Disch* array. If conditions #4 and #5 are both not met, then the changes performed in the last smoothing cycle involving the *Charge* and *Disch* array and

Table 1
Initial entries of the *Demand*, *Price*, *Charge*, *Disch* and *Q* arrays for the representative case.

Entries (i, r, m, u)	1	2	3	4	5	6	7	8	9	10	11	12	13	14	15	16	17	18	19	20	21	22	23	24
Demand, dem_i, kW	−6.8	−7.6	−7.9	−7.9	−7.9	−7.9	−7.9	1.3	10.7	5.7	7.0	−2.3	4.0	2.3	15.2	20.2	10.0	27.4	22.0	23.2	28.1	14.5	11.8	4.8
Price, $price_i$	1	1	1	1	1	1	1	1	1	1	1	1	1	1	1	1	1	1	2	2	1	1	1	1
Charge, $charge_{1.m}$, kW	−6.8	−7.6	−7.9	−7.9	−7.9	−7.9	−7.9	1.3	10.7	5.7	7.0	−2.3	4.0	2.3	15.2	20.2	10.0	27.4	0	0	28.1	14.5	11.8	4.8
Charge, $charge_{2.m}$	1	2	3	4	5	6	7	8	9	10	11	12	13	14	15	16	17	18	0	0	21	22	23	24
Disch, $disch_{1.u}$, kW	0	0	0	0	0	0	0	0	0	0	0	0	0	0	0	0	0	0	22.0	23.2	0	0	0	0
Disch, $disch_{2.u}$	0	0	0	0	0	0	0	0	0	0	0	0	0	0	0	0	0	0	19	20	0	0	0	0
Q, q_r, kWh	20	20	20	20	20	20	20	20	20	20	20	20	20	20	20	20	20	20	20	20	20	20	20	20

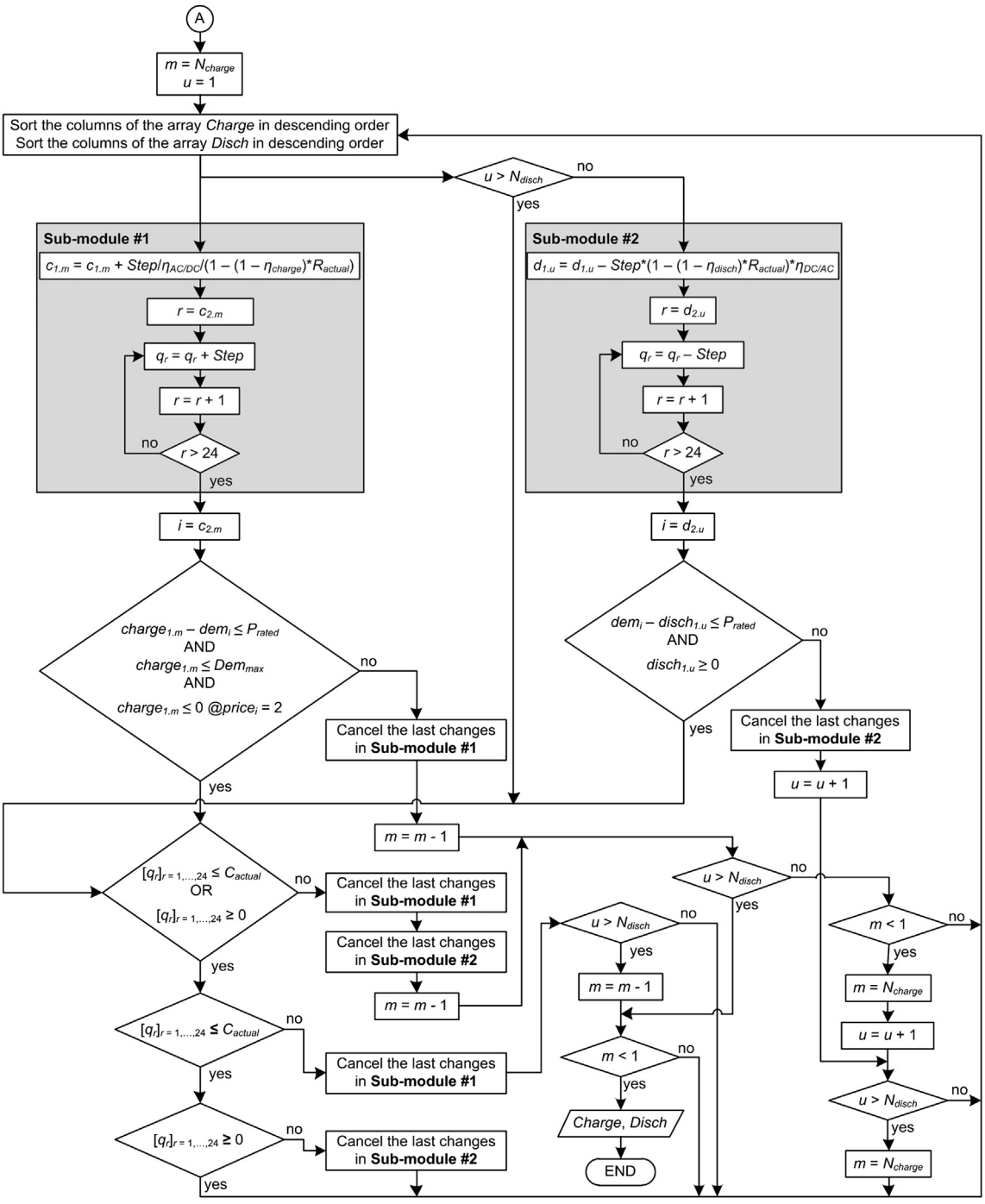

Fig. 3. Flowchart of battery system management model (part 2 of 2).

consequently the relevant entries in the *Q* array are cancelled. Then smoothing continues with the next lowest entry in the *Charge* array and with the same entry in the *Disch* array. However, if only condition #4 or #5 is not met, then the changes performed in the last smoothing cycle involving the *Charge* or *Disch* array respectively and consequently the relevant entries in the *Q* array are cancelled. Then smoothing continues with the same entries in the *Charge* and *Disch* arrays. This procedure continues until the conditions are met. If the conditions cannot be satisfied for all the entries in the *Charge* array, then smoothing continues with the next highest entry in the *Disch* array. If all the entries in the *Disch* array are checked and the conditions still cannot be satisfied, there is a check as to whether additional smoothing is possible for all entries in the *Charge* array. If no more smoothing is possible under the above conditions, the smoothing is completed.

The battery system's operating power until the end of the current hour is the difference between the initial residual demand (dem_1) and the smoothened residual demand in hour number one ($charge_{1.m}$ or $disch_{1.m}$). Battery SoC at the end of the first hour is fed into q_{actual} for the next calculation.

For the representative residual demand profile (see Fig. 2), applying a battery system with rated power of 8.9 kW and battery

Table 2
Final entries of the *Charge*, *Disch* and *Q* arrays for the representative case.

Entries (r, m, u)	1	2	3	4	5	6	7	8	9	10	11	12	13	14	15	16	17	18	19	20	21	22	23	24
Charge, $charge_{1,m}$, kW	21	18	16	23	22	15	24	9	17	10	8	11	13	14	12	1	2	6	3	4	5	7	0	0
Charge, $charge_{2,m}$	28.0	27.3	20.2	18.9	18.9	15.2	13.6	10.7	10.0	7.0	7.0	7.0	7.0	7.0	6.5	2.1	1.3	1.0	1.0	1.0	1.0	1.0	0	0
Disch, $disch_{1,u}$, kW	14.3	13.1	0	0	0	0	0	0	0	0	0	0	0	0	0	0	0	0	0	0	0	0	0	0
Disch, $disch_{2,u}$	20	19	0	0	0	0	0	0	0	0	0	0	0	0	0	0	0	0	0	0	0	0	0	0
Q, q_r, kWh	28.3	36.6	44.9	53.2	61.5	69.8	78.1	83.4	83.4	84.6	84.6	92.9	95.7	100	100	100	100	100	90.5	81.0	81.0	85.1	91.7	100

capacity of 100 kWh, the calculated *Charge*, *Disch* and *Q* arrays will be as in Table 2. The provisional residual demand profile for 24 h in advance can be obtained from the *Charge* and *Disch* arrays, where $charge_{1.m}$ and $disch_{1.u}$ contain residual demand values and $charge_{2.m}$ and $disch_{2.u}$ indicate the number of the hour. This profile is depicted in Fig. 2 as a dotted line. In this case, the optimal battery system operating power for the current hour is 8.9 kW. The *Q* array entries indicate battery SoC at the end of each hour. Battery SoC at the end of hour one is 28.3 kWh, which is the actual SoC for the next calculation (q_{actual}). The battery reaches its full charge capacity at the end of the low price period (at the end of hour 18), then it is discharged at full power during the high price period (hours 19 and 20) and fully charged again at the end of hour 24.

Since this calculation is based on prediction data, battery operating power can be adjusted in order to compensate prediction error. These changes in battery operation may lead to battery capacity being used differently from what was predicted. Actual battery use should therefore be registered and taken into account for the calculation of battery system operating power for the next hour.

After every charge-depleting cycle, the new battery capacity (C_{actual}) and internal resistance (R_{actual}) are calculated according to the battery aging characteristics in Ecker et al. [15], as described in Section 2.3.

2.2. Battery system efficiency

For an efficient and feasible operation, the battery system should provide high energy conversion efficiency. Efficiency depends mainly on the charging/discharging current and battery aging. The latter will be discussed in the next sub-section.

Charging/discharging current up to the rate of 1 C does not influence battery efficiency significantly [16]. At this current rate, efficiency stays in a range of 0.97–0.98. Higher currents, however, cause higher decreases in efficiency, which drops to around 0.89 at 10 C, for example. The effect of SoC on battery efficiency (change in internal resistance) is not considered in this study.

As full discharge is down to as low as 20% of full charge and the charging/discharging rate is 1 C, the full charge-depleting cycle of the battery (full discharged and charge) will be completed within 2 h. When applied for demand smoothing (peak shaving) purposes at distribution transformer level, the battery will contribute mainly by increasing off-peak demand during night hours (charging operation) and by peaks having during morning and evening peak demand periods (discharging operation). According to Purvins et al. [12], an aggregated statistical household daily demand profile has off-peak and peak demands of a duration of several hours each. Thus, for efficient demand smoothing, battery capacity (if sufficient) should be used for several hours in charging or discharging operation mode. So, if the battery contributes to peak demand shaving for more than one hour in total, the battery discharge rate will be lower than 1 C. Similarly, the battery charging rate is decreased during off-peak hours. The longer the period a battery is in one operation mode (charging or discharging), the lower the average current. Assuming that battery capacity is sufficient to contribute to peak demand shaving for more than one hour, it can be concluded that the battery's average rate of charge/discharge will be below 1 C. This is the current range in which the battery's charging/discharging efficiency can be assumed to be constant, between 0.97 and 0.98, i.e. 0.975.

The internal resistance of the battery can change at different charging/discharging current rates, especially at low cell temperatures of 10 °C and below [17]. Resistance is higher at low currents and decreases at high currents, e.g. at 1 C, resistance is around 1.5 times higher than at 3 C. However, at cell temperatures as high as

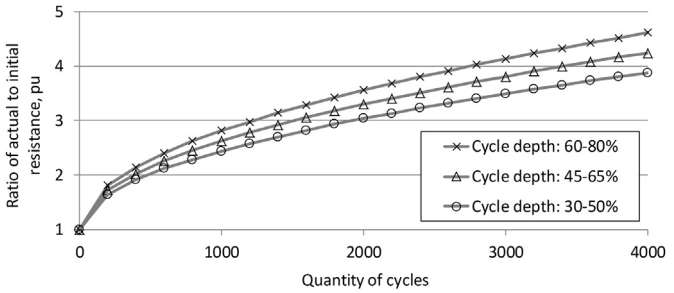

Fig. 4. Effect of aging on the internal resistance of the battery.

25 °C, current has a minor influence on resistance for new or aged batteries. This indicates that there is no significant loss of battery efficiency at operating currents close to zero. However, electrical-power converter efficiency drops rapidly, operating below 10% of its rated power [18]. Thus, the battery system's operation (instantaneous) power range is assumed to be 10–100% of rated power. Power converter efficiency does not vary significantly in this range and can be assumed to be 96% [18–20].

Deployment of distributed RES-E may change demand profile at distribution transformer level. This in turn may change battery operation profiles: the number of charge-depleting cycles and the depth of charge. High photovoltaic (PV) system deployment will not lead to a full charge-depleting cycle shorter than one day at distribution transformer level [12]. On the other hand, wind turbines could bring hourly power variations in the electricity system, which require high power damping and battery operation at high charge/discharge rates (>1 C).

2.3. Battery aging

Aging is an important factor in the feasible utilisation of batteries since it affects battery performance by reducing capacity and increasing internal resistance. The latter is directly proportional to energy losses in battery charging and discharging. Degradation of battery performance is strongly influenced by the way the battery is exploited: the number and depth of charge-depleting cycles. Each charge-depleting cycle reduces available battery capacity. The effect of different temperatures on battery aging (change of capacity and internal resistance) is not taken into account in this study. Cell temperature is assumed to be constant at 40 °C.

The increase of internal battery resistance and reduction of battery capacity due to battery aging is studied by Ecker et al. [15] and depicted in Figs. 4 and 5 respectively. Numbers of cycles on the horizontal axis are synchronised with capacity reduction so that 50% capacity reduction occurs after 4000 deep cycles [21]. Curves

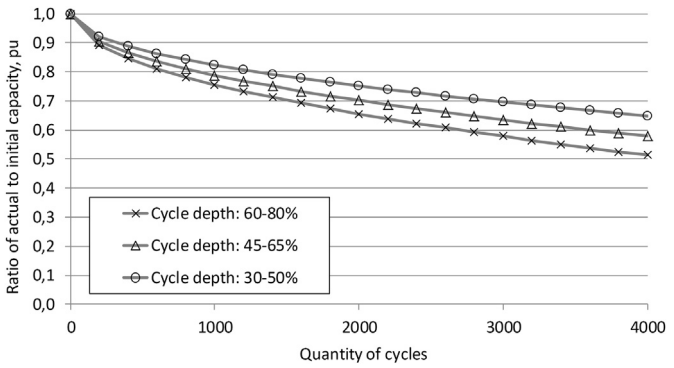

Fig. 5. Effect of aging on the capacity of the battery.

presented in these figures can be expressed as quadratic mathematical functions and applied in the battery management model. On the basis of the actual internal resistance or actual capacity of the battery, the graph shows how much resistance will rise after additional charge-depleting cycles. The battery's internal resistance (R) and capacity (C) as a function of the number of charge-depleting cycles can be expressed as follows:

$$R = 1 + \mathrm{SQRT}(N)/x \quad (1)$$

$$C = 1 - \mathrm{SQRT}(N)/x \quad (2)$$

where N is the number of charge-depleting cycles and x is a shape factor. The shape factor for the resistance curve is 17.5 for cycle depth of 60–80%, 19.5 for cycle depth of 45–65% and 22 for cycle depth of 30–50%. The shape factor for the capacity curve is 130 for cycle depth of 60–80%, 150 for cycle depth of 45–65% and 180 for cycle depth of 30–50%.

3. Case study: Great Britain

Great Britain is chosen as a hypothetical case study for testing the proposed battery management model. The battery system is applied at distribution grid level. The study time horizon is 2020. This section includes a methodology on the acquisition of demand profiles and wind speed data in the distribution grid and on a national scale; calculation of wind turbine and wind farm power; calculation of price profile and battery system sizing. The section concludes with results.

3.1. Distribution grid

This sub-section describes the acquisition of the demand profile and wind speed data at distribution grid level, as well as the calculation of wind turbine power.

3.1.1. Demand

Demand profiles in the distribution grid are generated using the domestic electricity consumption model developed by Richardson et al. [22]. This model is based on a combination of patterns of active occupancy (i.e. when people are at home and awake) and daily activity profiles that characterise how people spend their time performing certain activities. The model covers major appliances. Lighting loads follow seasonal daylight variations. The model has been validated using statistical data from households over one year in the East Midlands region of the UK, which show characteristics similar to those of the modelled demand profiles.

In this study, an aggregated demand of 25 randomly generated profiles of households with three residents per house is used as the distribution grid demand. The model generates different daily demand profiles for each month taking account of seasonal demand characteristics. Each month has its specific working day and weekend demand profile. In the present study, aggregated working day profiles for one month are assumed to be the same. The same applies to weekend profiles. The resulting hourly distribution grid demand profile for the first seven days in January is depicted in Fig. 6. Working days and weekends are arranged as for the first seven days of January 2011, i.e. starting from Saturday. This is because in the next sub-section the statistical demand recorded for 2011 is used as the aggregated annual demand profile for Great Britain.

In Fig. 6 it is noticeable that weekend peak demand (28 kW) is slightly higher than peak demand on weekdays (25 kW) in January. During night hours, demand drops to near zero. Short off-peak

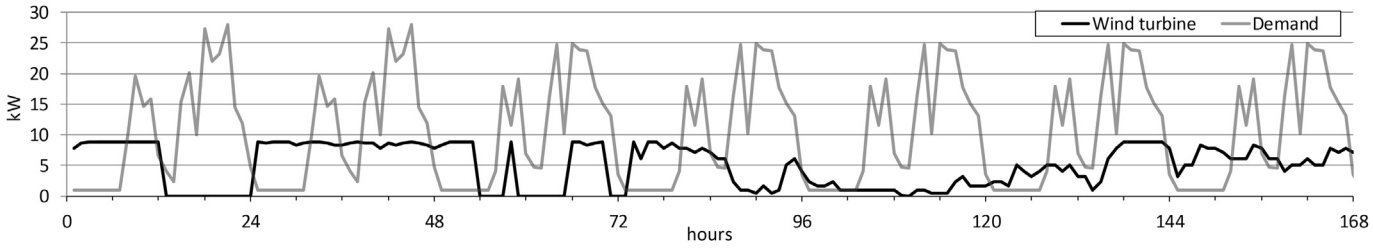

Fig. 6. Distribution grid demand and wind turbine generation curves for the first seven days of January.

demand occurs in the afternoon between morning and evening peak demands.

The histogram of annual distribution grid demand in Fig. 7 shows the probability of occurrences for different demand values. For example, low demand up to 5 kW may occur in 32 h out of 100.

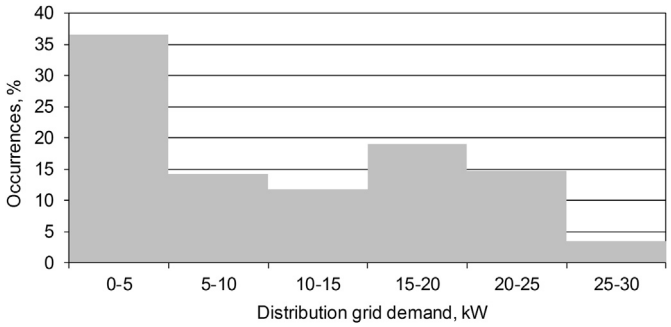

Fig. 7. Histogram of yearly distribution grid demand.

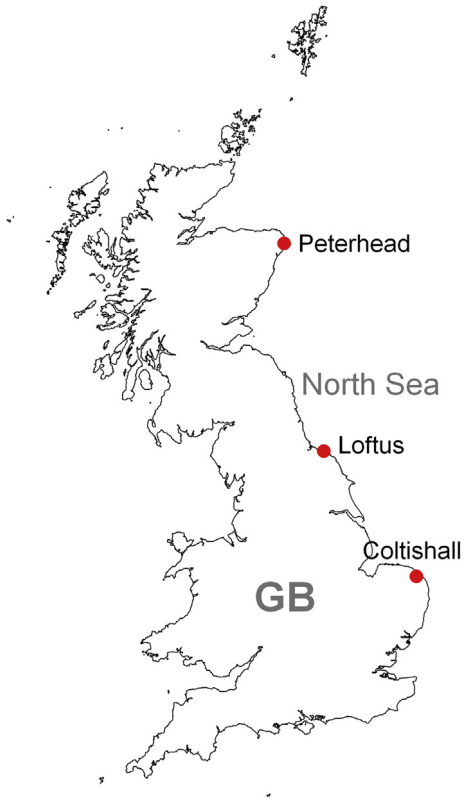

Fig. 8. Wind farm sites in Great Britain—Peterhead in Scotland, Loftus in North East England and Coltishall in East Anglia.

These low demand hours are the times when RES-E generation is most likely to cause power surplus. Other demand values up to 25 kW have occurrence probability in a range of 12 to 19%. Maximum annual demand is 29.7 kW.

3.1.2. Wind turbine

The location of the distribution grid is assumed to be in Peterhead in Scotland (see Fig. 8), which is characterised by relatively high wind speeds. One wind turbine is considered to be installed in the distribution grid in question, the size of which varies according to scenarios described below. Wind data are statistical hourly wind speeds obtained from the UK Meteorological Office [23] and include time series at an altitude of 10 m recorded in 1998.

Hub height is assumed to be 100 m and wind turbine availability 100%. Wind speed at 100 m altitude is calculated following the methodology described in previous work by Purvins et al. [24]. The wind turbine power curve (Fig. 9) is obtained from IEC [25]. The operating power of the wind turbine is calculated according to this curve.

The annual distribution of calculated wind turbine operating power in relative values is presented in Fig. 10. For 17% of the time, wind farm generation is close to its maximum. Low wind farm output, up to 10% of the rated power, occurs on around 13 days out of 100. The first column (0–10) also includes days when the wind farm is idle (does not produce any power): 17 days out of 100. The annual wind farm capacity factor is relatively high: 0.40.

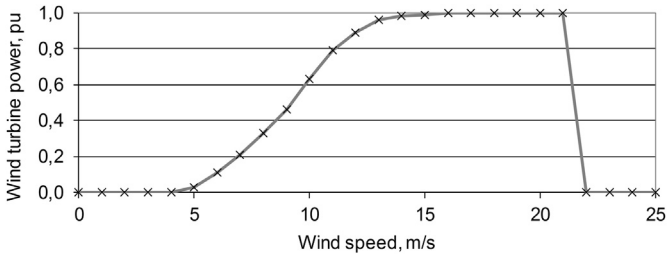

Fig. 9. Wind turbine power curve [25].

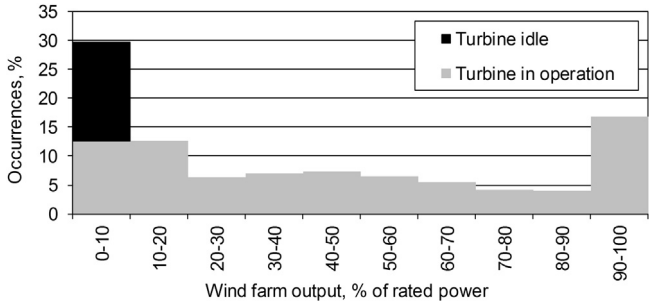

Fig. 10. Histogram of yearly wind turbine power output.

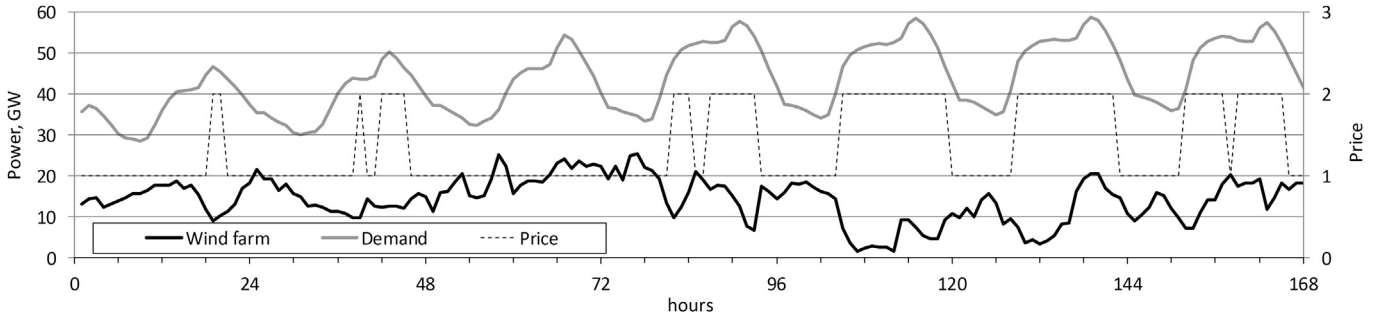

Fig. 11. Aggregated GB demand, aggregated GB wind generation and electricity price curves for the first seven days of January 2020.

3.2. Electricity price curve

Since wind farms are the main contributors to RES-E in 2020, the electricity price curve is calculated using total GB electricity demand and aggregated wind farm production profiles. Two electricity prices are assumed: high and low price. High price is during hours when residual demand is above average residual monthly demand and low price during hours when it is below.

Aggregated hourly GB demand values are obtained from the ENTSO-E statistical database [26] for 2011. For the 2020 scenario, the 2011 annual demand profile is assumed to increase in proportion to the increase in total electricity consumption in Great Britain between 2011 and 2020. According to the national renewable energy action plan [14], this increase is 6.9%. The resulting demand profile is shown in Fig. 11. As compared with distribution grid demand (Fig. 6), aggregated GB demand is smoother and minimum GB demand well over the average, as seen in Fig. 12. Higher GB peak demand occurs during working days.

Aggregated wind farm generation is obtained from three nearshore wind farm locations along the east coast of Great Britain: Peterhead in Scotland, Loftus in North East England and Coltishall in East Anglia. It is considered that wind farm capacity of 27.9 GW is spread equally between offshore and onshore at each wind farm site, which is roughly the resulting proportion for 2020 [14]. As for the previous sub-section, hourly wind speed data are obtained from the UK Meteorological Office database [23] at an altitude of 10 m as recorded in 1998. All wind turbines in the wind farms are assumed to have a hub height of 100 m. The new high wind speed is calculated according to the method presented by Purvins et al. [24]. The wind farm operating power calculation follows the projected wind farm regional profiles from the TradeWind study [27], which provides offshore and onshore wind farm power curves for 2008 and 2030. Power curves for 2020 obtained using linear interpolation between these two curves are presented in Fig. 13. According to these power curves, maximum operating power is 89% of rated (installed) power for an aggregated offshore wind farm and 94% for an onshore wind farm. An aggregated wind farm capacity of 27.9 MW is taken and it is assumed that the wind farm capacity is spread equally over the three sites. Wind farm operating power is calculated separately for each site.

The annual distribution of aggregated wind farm operating power in relative values is presented in Fig. 14. Because it is aggregated, total power practically never reaches zero. The probability of high wind power output at all the sites is very low: wind farm output of 80–90% from the installed capacity occurs on only two days out of 100. This effect is due to the spatial aggregation of wind farms/turbines, as studied previously by Purvins et al. [28].

Since the annual aggregated GB demand and the wind farm production profiles have been obtained, the electricity price curve can be calculated as depicted in Fig. 11. Low and high price periods change from day to day due to high wind farm penetration in the electricity system. On the first day of January, the high price applies for only two hours (19 and 20) during evening peak demand. For the rest of the day, the electricity price is low because of high wind farm generation. High wind farm generation can lead to low prices even during peak demand, e.g. on the third day (hours 49–72), when the electricity price is low in all hours.

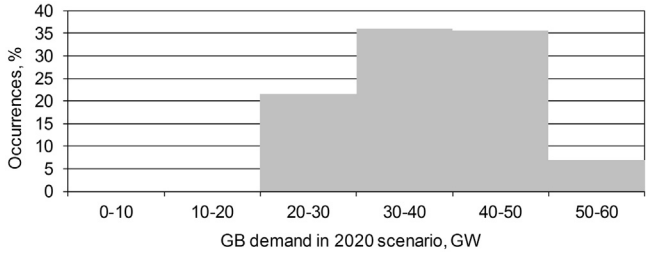

Fig. 12. Histogram of aggregated yearly GB demand.

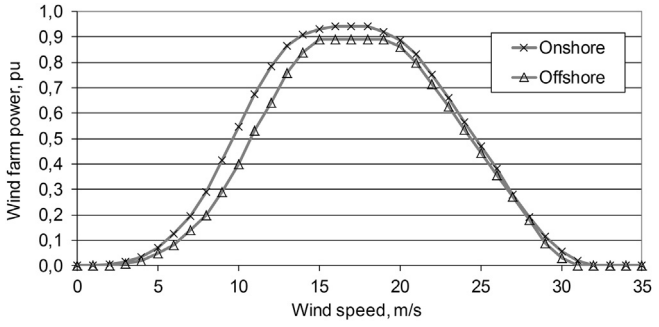

Fig. 13. Regional wind farm power curve – offshore and onshore [27].

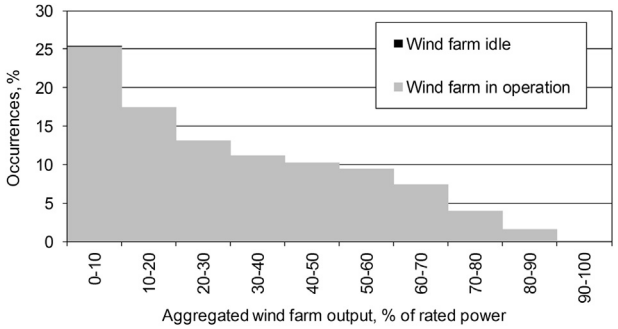

Fig. 14. Histogram of aggregated yearly GB wind farm production.

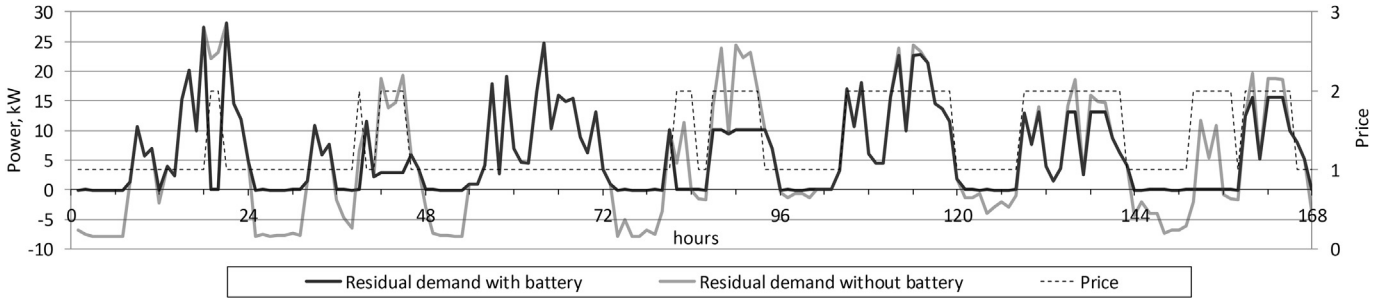

Fig. 15. Residual distribution grid demand curves with and without battery for the first seven days of January – battery applied only for energy surplus compensation.

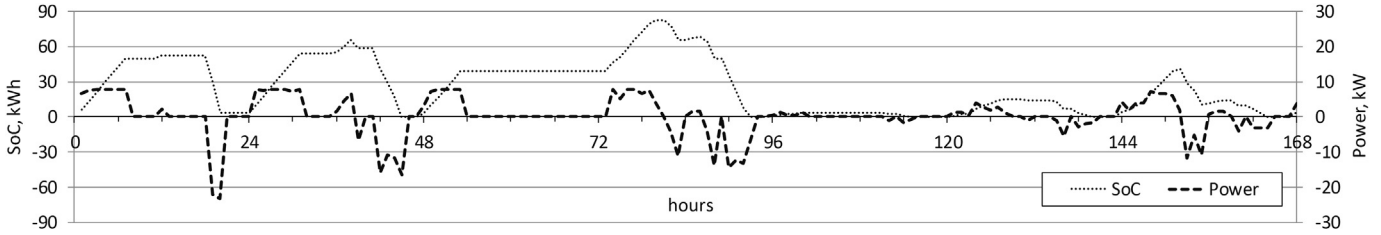

Fig. 16. Battery system power and battery SoC for the first seven days of January – battery applied only for energy surplus compensation.

3.3. Battery system sizing

This section provides the methodology for battery sizing. The minimum battery capacity is determined by the need to compensate wind turbine generation surplus in the distribution grid in order to prevent reverse power flows in the distribution grid transformer. Scenarios with different wind turbine sizes are examined: 10, 15, 20, 25 and 30% of the annual peak demand in the distribution grid.

Minimum battery capacity is calculated using the battery management model presented in Section 2.1. For battery sizing purposes, battery capacity and battery system rated power are assumed to be unlimited. The battery is applied only for storing wind energy surplus, so it is charged during hours of negative residual demand. In the rest of the hours of high electricity price, the battery operates in discharging mode where possible and supplies stored energy to the grid. Battery capacity is thus used only for wind power surplus compensation. No constraints are applied for the prediction period, so the annual profiles for residual demand and electricity price are known in advance. Battery system efficiency for this calculation is assumed to be equal to that of a new battery system. The degradation of battery parameters (i.e. reduction of capacity and efficiency) due to aging is not taken into account. The aging effect would be taken into account in battery installation, i.e. the capacity of the installation should be slightly higher than that used for the calculations in order to cover battery degradation.

The battery sizing process for a representative case (in the first seven days of January) is illustrated in Figs. 15 and 16. The residual demand is a product of the aggregated distribution grid demand minus wind turbine generation. Wind turbine size in the representative scenario is 8.9 kW (30% of annual distribution grid peak demand). Fig. 15 depicts the residual distribution grid demand profiles before and after applying the battery. All the negative residual demand values are compensated with battery and high electricity price periods are used to discharge the battery. Fig. 16 represents the battery's SoC and battery system operating power. Positive power values indicate that the battery is in charging mode, whereas negative power indicates discharging mode. The battery's minimum SoC in Fig. 16 is set to zero, since it is unknown as a result of applying unlimited battery capacity. The number of cycles and the required capacity are obtained from the SoC curve. A cycle is counted every time the battery changes its operation from discharging to charging mode. The battery capacity is then equal to the amount of energy stored in the battery during this cycle. For example, in the first 48 h in order to compensate negative residual demand, the battery performs two charge-depleting cycles. The required capacities in the first and second cycles are 50 and 62 kWh respectively. This is the capacity which should be available in the battery. In reality, the actual battery capacity will be higher because of minimum SoC constraints, e.g. 20%.

The distribution of required battery capacities (i.e. the minimum capacity to theoretically compensate the wind power surplus) for different wind turbine sizes is shown in Fig. 17. The capacity presented is actual capacity, where the minimum battery discharge of 20% of rated capacity is taken into account. Fig. 17 shows the number of cycles for which a specific battery capacity is required over one year. For example, at wind turbine size of 10% (as a percentage of the maximum annual demand in the distribution grid), the battery of 10 kWh is enough to compensate wind power surplus in 125 cycles per year. However, this capacity is not enough to compensate surplus power in the rest of the cycles. Higher capacity (up to 20 kWh) is required for 41 additional cycles. Theoretically, therefore, in order to compensate most of the annual wind power surplus at 10% wind penetration,[4] the required battery capacity is 20 kWh. A bigger wind turbine leads to a higher power surplus. This consequently increases the required battery capacities. At a wind farm size covering 30% of the annual distribution grid peak demand, a battery capacity of 80 kWh is required in order to compensate most of the wind power surplus. Still, several cycles require higher capacities (up to 330 kWh). These are critical cases of low electricity price periods for several days while wind turbine production is high.

[4] Penetration refers to the wind turbine size as a percentage of maximum annual demand in the distribution grid.

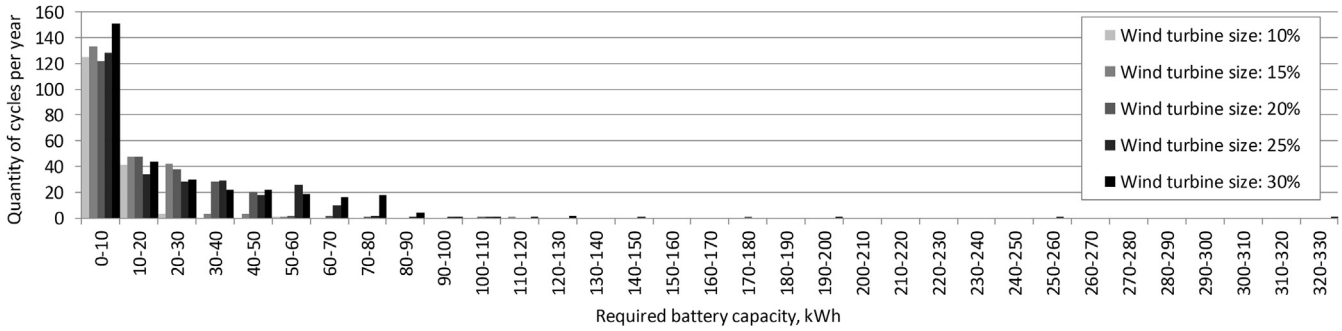

Fig. 17. Histogram of required annual battery capacity at different wind turbine sizes in the distribution grid as a percentage of maximum annual distribution grid demand – battery applied only for energy surplus compensation.

3.3.1. Scenarios

Optimal battery capacity can be obtained from the battery sizing results. These capacities, for different wind turbine sizes, are presented in Table 3. The capacity values chosen are slightly higher than the theoretical capacity needed for compensating most of the wind power surplus. This assumption is based on decreases in battery capacity and efficiency caused by battery aging (see Section 2.3). For example, the battery capacity chosen in Scenario #5 (wind turbine size of 30% of maximum annual demand in the distribution grid) is 100 kWh, whereas the theoretical required capacity is 80 kWh. Battery system rated power is assumed to be equal to installed wind turbine power capacity in the distribution grids. So, with sufficient battery capacity, the battery system will be able to store wind energy surplus at low demand and high wind turbine generation. However, limited rated power of the battery system and short periods of high electricity price may limit battery discharge.

3.4. Results

Results are presented for the five scenarios described in the previous sub-section. The battery system is managed according to the management model in Section 2.1. Fig. 18 shows how much of the wind energy surplus is stored in the battery and how much of the energy surplus the battery system was not able to compensate. For example, in Scenario #5 (at wind turbine size of 30% of annual peak demand) 7 MWh out of 7.9 MWh of wind energy surplus is stored in the battery. Not only limited battery capacity, but also limited battery system power and management constraints (i.e. limited residual demand and electricity price prediction period) influence the performance of the battery system. Energy surplus not stored may increase in subsequent years due to battery aging.

The effect of these limits is depicted in Fig. 19, which shows a representative residual demand curve for the first seven days in January in Scenario #5 (first two days are a weekend). This includes the electricity price curve, as well as residual demand with applied battery system. The residual demand curve applying the battery is slightly smoothed: a significant amount of wind energy surplus is stored in the battery, residual peak demand is reduced during times of low electricity price and off-peak demand increased at low price. In the first few hours, 1–6, the battery is able to compensate the entire wind power surplus. However, in later hours, 7 and 25–31, negative residual demand remains, which indicates that the battery is not capable of storing all the energy surplus. This is due to the limited battery system parameters and battery management constraints. When the battery operation mode and battery system operating power is calculated for the first hour in January (hour 1), the battery management model does not have information on wind energy surplus during hours 25–31, because the prediction period is limited to 24 h. The battery system's operating power in the first hour is therefore set to maximum (rated power), which is 9.8 kW. This is an optimal operating power in line with the three management priorities (see Section 2).

The calculation results for hour one are illustrated in Fig. 19 as a dotted line (detailed curves provided in Fig. 2). As explained above, only the optimal battery system power calculated for the first hour will be applied in the battery system. Calculation results for the other hours (2–24) are provisional and will be updated and recalculated at the beginning of every subsequent hour. Energy surplus during the first few hours (1–7) is stored in the battery. During these hours, the battery system operates at rated power (8.9 kW), leading to an off-peak residual demand increase slightly above zero. The excess battery capacity is used in the rest of the hours of the low electricity price period, in which the battery reaches full charge. During the two high price hours (19 and 20), the battery is in discharging operation at full power. In the last few hours, 22–24, the battery is charged again and reaches its full charge at the end of hour 24. As a result, energy surplus is stored in the battery, battery utilisation reaches its maximum and residual demand is smoothed when possible. The highest residual demand during times of high electricity price is reduced and the lowest residual demand during low price periods is increased using the available battery system resource.

Table 3
Scenarios for different wind farm sizes in the distribution grid.

Scenarios	Wind turbine		Battery system	
	Penetration (%)	Rated power (kW)	Capacity (kWh)	Rated power (kW)
1	10	3.0	25	3.0
2	15	4.5	40	4.5
3	20	5.9	65	5.9
4	25	7.4	90	7.4
5	30	8.9	100	8.9

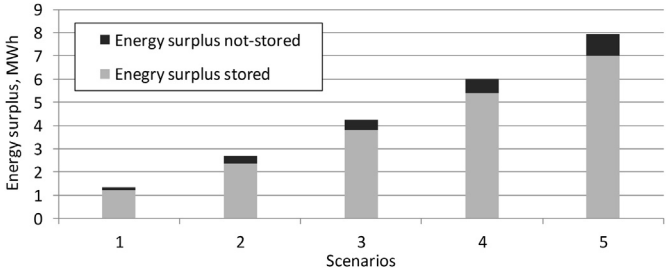

Fig. 18. Annual stored and not stored wind energy surplus at different wind turbine sizes in the distribution grid.

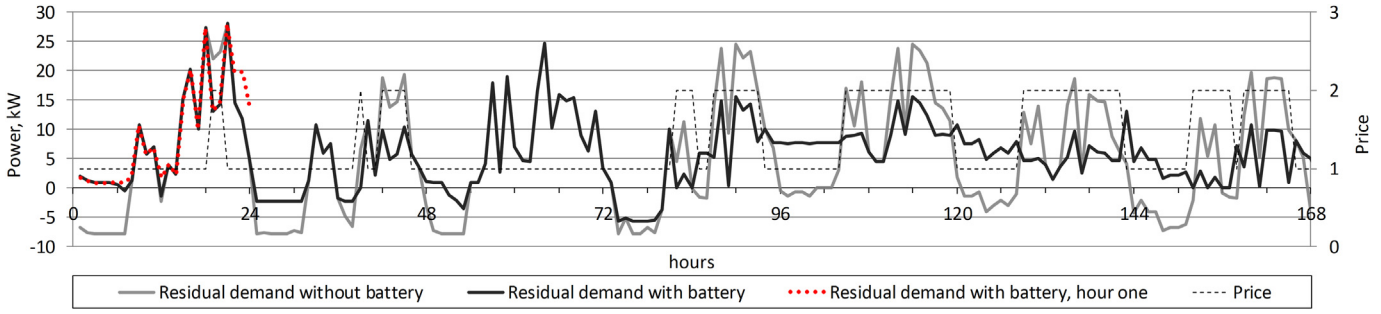

Fig. 19. Residual distribution grid demand curves with and without battery system and price curve for the first seven days of January.

When calculating optimal operating conditions for the battery system for further hours, the management model receives predicted information about negative residual demand starting from hour 25. As a result, wind surplus is not compensated completely during hour 7, because part of the battery capacity is reserved for compensating wind surplus during hours 25–31.

Another limitation is battery system rated power, which limits battery discharge during high electricity price hours (19 and 20). Residual demand is smoothed when possible. However, residual demand peaks remain during high electricity price times, e.g. hours 18 and 21.

Battery SoC and the operating power of the battery system are depicted in Fig. 20. This shows that, where possible, battery SoC reaches 100 kWh, which is the maximum battery capacity. During high electricity price periods without wind energy surplus, the battery supplies as much energy to the grid as possible. It is thus prepared for the next charging cycle. It is never in discharging mode when the electricity price is low, which causes high wind energy surplus during hours 74–80 (Fig. 19).

The histogram of annual battery utilisation applying the proposed management model and representing the results of Scenario #5 (see Fig. 21) shows the minimum required battery capacity (in black), which theoretically covers all wind power surplus as presented previously in Fig. 17. The lighter coloured columns show battery utilisation in Scenario #5 (battery system rated power of 8.9 kW and battery capacity of 100 kWh). The figure shows that battery capacity of a range of 50–100 kWh is highly utilised in a total of 263 cycles, in which the cycle depth is close to 30–80% of the rated battery capacity. In the rest of the charge-depleting cycles (188), battery utilisation is lower. Fig. 21 indicates that the proposed approach to battery management increases battery utilisation efficiently as compared with management where the battery is applied only for storing energy surplus.

Battery utilisation (cycle depth and number of cycles) for each of the five scenarios is illustrated in Fig. 22. Utilisation is expressed in per unit values, where the base unit is a full cycle of a new battery system. In other words, the sum of depth of charge is calculated for all cycles per year and divided by the full cycle capacity of the new battery. For example, in Scenario #5 the full cycle capacity of a new battery is 80 kWh, assuming a 20% minimum state of charge. These results will be used in the next section for calculating the payback period of the battery system. Results indicate that the number of cycles equivalent to the full cycle of a new battery varies between 216 and 253 in the first year of battery utilisation for the five scenarios. In subsequent years of battery operation, this number will decrease slightly due to battery aging. In Scenario #5, for example,

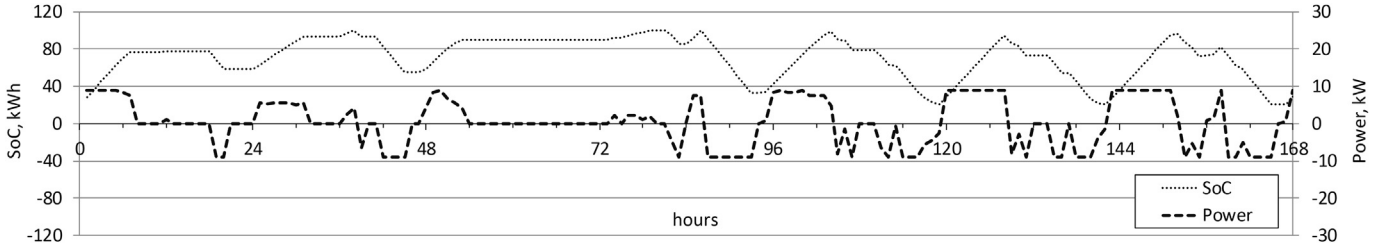

Fig. 20. Battery system power and battery SoC curves for the first seven days of January

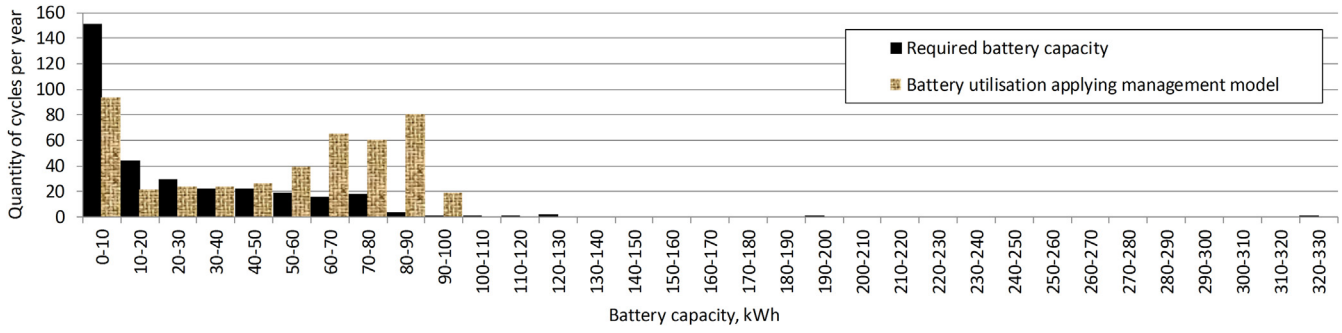

Fig. 21. Histogram of required annual battery capacity and resulting annual battery utilisation applying battery management model in Scenario #5.

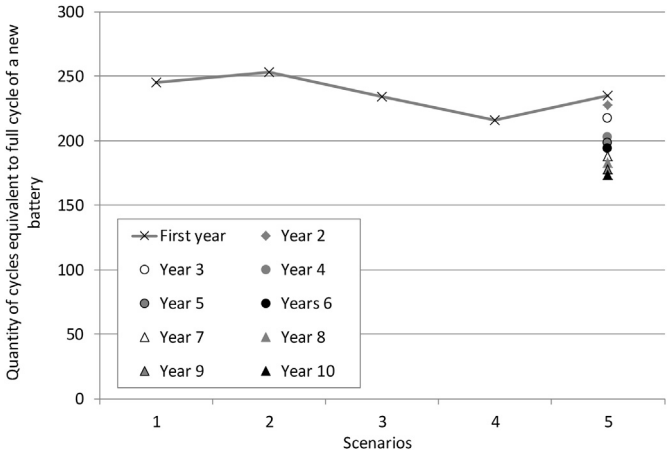

Fig. 22. Annual battery utilisation for different wind turbine sizes in the distribution grid.

it drops from 235 to 174 in the first and tenth year respectively. Energy surplus not stored increases due to battery aging in subsequent years of battery operation, as shown in Fig. 23 for Scenario #5. The energy surplus not stored increases to 1.6 MWh in the tenth year, whereas in the first year it was as low as 0.9 MWh.

The effect of aging on the internal resistance and available battery capacity is represented in Figs. 24 and 25 respectively. This is expressed in per unit values, with the base unit the new battery's capacity and internal resistance respectively (vertical axes). The modelling results show trends for the degradation of battery parameters due to aging similar to those in Figs. 4 and 5. Battery aging is faster for new batteries and slows down during battery exploitation.

4. Feasibility

The feasibility of battery system implementation in electricity distribution grids can be assessed from different points of view: those of the end users, distribution system operators and electricity market players. The feasibility of using battery systems for residual household-demand smoothing from the end-user side can be roughly calculated from the lifecycle cost (including capital and operating costs) and benefits due to electricity price elasticity in battery charging and discharging periods. Furthermore, at distribution grid level, other technical benefits due to residual demand smoothing (and peak shaving), such as the increased capacity factor of power-transfer corridors and of conventional power generators, and higher security of energy supply should be considered when carrying out feasibility studies for battery systems. Electricity market players could also be beneficiaries where battery systems can provide back-up power and/or balance variable generation

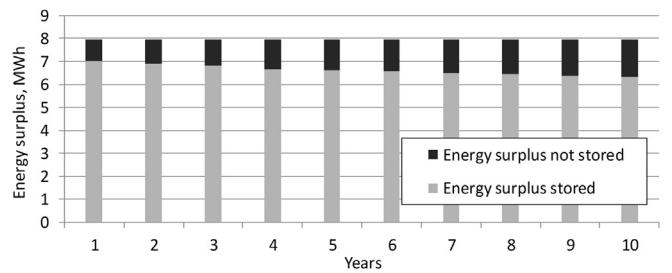

Fig. 23. Stored and not stored wind energy surplus for 10 years – Scenario #5.

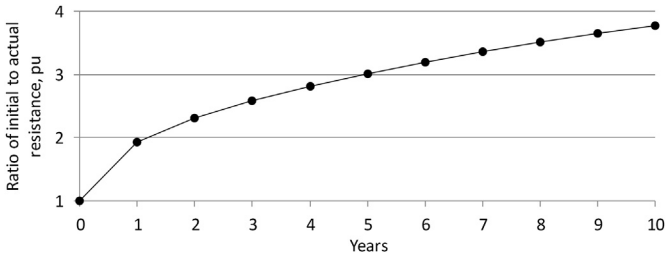

Fig. 24. Increase of battery's internal resistance for ten years for Scenario #5.

from renewable energy sources like wind farms. Some conventional power reserves could be replaced by battery based storage systems.

In this section, economic benefits are calculated from the end-user side. Quantification of other benefits is beyond the scope of this study. Input parameters for this calculation are battery system efficiency, system capital cost, the value of low electricity price ($Price_{min}$ assumed equal to 0.15 EUR/kWh) and payback period (assumed in a range of 1000–2500 full charge-depleting cycles). Battery aging is not taken into account. Cycle efficiency is assumed equal to the efficiency of a new battery.

$$\eta = \eta_{AC/DC}{}^{*}\eta_{charge}{}^{*}\eta_{disch}{}^{*}\eta_{DC/AC} = 0.96{*}0.975{*}0.975{*}0.96 = 0.88 \quad (3)$$

The outcome of this calculation is the required value of high electricity price, which will lead to the specific payback period in cycles, calculated as follows:

$$Price_{max} = (\mathrm{CAPEX}/N + 0.8{*}Price_{min})/(0.8{*}\eta) \quad (4)$$

where CAPEX is the capital cost of the battery system in EUR/kWh and N is the payback period in number of cycles (full cycles of a new battery). Factor 0.8 indicates that available battery capacity is 80% of the battery's rated capacity (at minimum SoC of 20%).

As a result, the required value of high electricity price as a function of capital cost and payback period in cycles is shown in Fig. 26. A lower number of full cycles in the payback period requires a higher value of high electricity price. For example, in the case of a battery system with CAPEX of EUR 300/kWh, the payback period of 2000 cycles requires a high electricity price of at least EUR 0.38/kWh, whereas a payback period of 1500 cycles requires a high electricity price of EUR 0.45/kWh. Similarly, knowing the value of high electricity price enables us to calculate the payback period, e.g. at CAPEX of EUR 500/kWh and high electricity price of EUR 0.45/

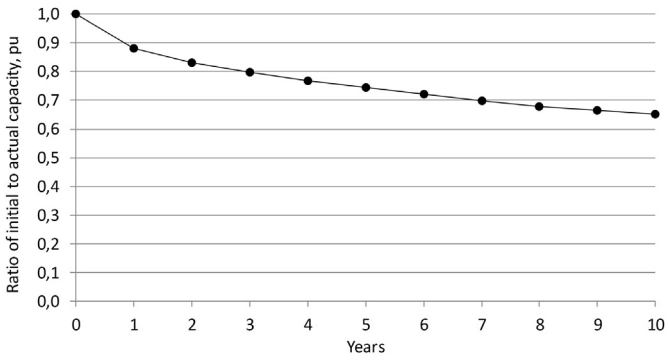

Fig. 25. Reduction of battery capacity for ten years for Scenario #5.

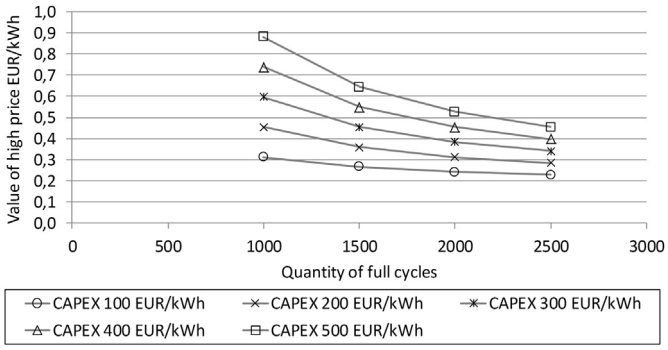

Fig. 26. Payback period in cycles as a function of high electricity price for different capital costs of battery system.

kWh, the payback period will be 2500 cycles. The necessary value of high electricity price depends more on the number of payback cycles at high CAPEX, due to the need for a higher difference between high and low electricity prices.

Furthermore, the results in this section can be used to calculate the payback period in years. For this purpose, the results from the case study in Section 3.4 (Fig. 22) are applied. These indicate the annual number of cycles equivalent to the full cycle of a new battery. In Scenario #5, the annual number of full charge equivalent cycles is 235 in the first year of battery utilisation (Fig. 22). The payback period can be obtained from Fig. 26. For example, a payback period of 2000 full charge cycles will be reached in around 10 years. In this calculation, the reduction of battery capacity due to battery aging is taken into account.

5. Conclusions

This article presents an optimal battery system management model for Lithium-ion battery system for stationary applications in distribution grids. The proposed model is based on three management priorities, the first being the maximum utilisation of RES-E energy in distribution grids, followed by efficient battery utilisation and residual distribution grid demand smoothing.

The model was applied for battery management in a distribution grid with 25 households and one installed wind turbine in a hypothetical case study in Great Britain in 2020. The battery capacity chosen for the case study was theoretically sufficient to cover most of the wind turbine energy surplus in the distribution grid. Modelling results show that the battery can contribute significantly to storing energy surplus (storing 87–90% of annual surplus with different wind turbine sizes) and reach efficient utilisation. Utilisation is measured in per unit values, where the base unit is a full charge-depleting cycle of a new battery system (80% of the capacity of a new battery). Results indicate that the number of cycles equivalent to the full cycle of a new battery varies between 216 and 253 in the first year of battery utilisation for different wind farm sizes. Efficient utilisation of the battery system is vital in keeping the payback period as short as possible. Some energy surplus is not stored as a result of limited battery capacity, battery system power and management constraints (i.e. limited residual demand and electricity price prediction period). Residual distribution grid demand (demand minus wind turbine generation) is smoothed when possible. However, the proposed management approach is not efficient in peak demand shaving in distribution grids, since the battery is not charged during hours of peak demand and low electricity price.

The proposed management model can be applied for any other distribution grids with various combinations of RES-E and different demand properties, as well as for different electricity price curves. The latter determine the battery's contribution to residual demand smoothing at electricity market level (in the case study: Great Britain). Thus efficient battery utilisation leads to a shorter payback period and a greater contribution to residual demand smoothing at electricity market level. Additional grid support services like frequency and voltage control can be applied in conjunction with the proposed battery management approach.

References

[1] K.C. Divya, J. Østergaard, Electr. Power Syst. Res. 79 (2009) 511–520.
[2] M. Beaudin, H. Zareipour, A. Schellenberglabe, W. Rosehart, Energy Sustain. Dev. 14 (2010) 302–314.
[3] Commission of the European Communities, http://eur-lex.europa.eu/LexUriServ/LexUriServ.do?uri=SEC:2009:1295:FIN:EN:PDF (consulted Feb. 2013).
[4] C. Wadia, P. Albertus, V. Srinivasan, J. Power Sources 196 (2011) 1593–1598.
[5] J. Leadbetter, L.G. Swan, J. Power Sources 216 (2012) 376–386.
[6] C.D. White, K.M. Zhang, J. Power Sources 196 (2011) 3972–3980.
[7] P. Denholm, M. Kuss, R.M. Margolis, J. Power Sources 236 (2013) 350–356.
[8] C. Ahn, C.T. Li, H. Peng, J. Power Sources 196 (2011) 10369–10379.
[9] I.T. Papaioannou, A. Purvins, E. Tzimas, Int. J. Electr. Power Energy Syst. 44 (2013) 540–546.
[10] J. Neubauer, A. Pesaran, J. Power Sources 196 (2011) 10351–10358.
[11] European Commission C(2012) 4536. http://ec.europa.eu/research/participants/portalplus/static/docs/calls/fp7/common/32765-annex_8_to_the_decision_energy_for_cap_en.pdf, 2012 (consulted Feb. 2013).
[12] A. Purvins, I.T. Papaioannou, L. Debarberis, Energy Convers. Manag. 65 (2013) 272–284.
[13] EWEA. http://www.ewea.org/fileadmin/files/library/publications/reports/EWEA_Annual_Report_2011.pdf, 2011 (consulted Feb. 2013).
[14] L.W.M. Beurskens, M. Hekkenberg, P. Vethman. http://www.ecn.nl/publications/PdfFetch.aspx?nr=ECN-E-10-069, 2011 (consulted Feb. 2013).
[15] M. Ecker, J.B. Gerschler, J. Vogel, S. Käbitz, F. Hust, P. Dechent, D.U. Sauer, J. Power Sources 215 (2012) 248–257.
[16] E.M. Krieger, C.B. Arnold, J. Power Sources 210 (2012) 286–291.
[17] W. Waag, S. Käbitz, D.U. Sauer, Appl. Energy 102 (2013) 885–897.
[18] J. Madouh, N.A. Ahmed, A.M. Al-Kandari, Int. J. Electr. Power Energy Syst. 43 (2012) 280–289.
[19] H. Qian, J.S. Lai, J. Zhang, W. Yu, Conference: Energy Conversion Congress and Exposition (ECCE), IEEE, 2010 3224–3229.
[20] T.F. Wu, K.H. Sun, C.L. Kuo, M.S. Yang, R.C. Chang, Conference: Energy Conversion Congress and Exposition (ECCE), IEEE, 2010 45–52.
[21] C. Rosenkranz, (Johnson Controls) at EVS 20, Long Beach, CA, November 15–19, 2003.
[22] I. Richardson, M. Thomson, D. Infield, C. Clifford, Energy Build. 42 (2010) 1878–1887.
[23] UK Meteorological Office, NCAS British Atmospheric Data Centre, http://badc.nerc.ac.uk/view/badc.nerc.ac.uk__ATOM__dataent_ukmo-midas (consulted Feb. 2013).
[24] A. Purvins, I.T. Papaioannou, I. Oleinikova, E. Tzimas, Energy 43 (2012) 225–236.
[25] IEC, 2005 IEC 61400-12-1: 2005(E) Wind turbines Part 12–1.
[26] ENTSO-E, https://www.entsoe.eu/resources/data-portal/consumption/ (consulted Feb. 2013).
[27] J.R. McLean, TradeWind. http://www.trade-wind.eu/fileadmin/documents/publications/D2.4_Equivalent_Wind_Power_Curves_11914bt02c.pdf, 2008 (consulted Feb. 2013).
[28] A. Purvins, A. Zubaryeva, M. Llorente, E. Tzimas, A. Mercier, Appl. Energy 88 (2011) 1461–1469.